Arabian Journal of Chemistry (2023) **16**, 104498

King Saud University

Arabian Journal of Chemistry

www.ksu.edu.sa
www.sciencedirect.com

ORIGINAL ARTICLE

Selective recovery of lanthanum from magnesium-containing solution via phosphoric acid modified kaolin prepared by a simple mechanochemical process

Kaibo Hu [a,b,*], Chanqi Zhang [b], Tianci Chen [b], Ke Li [a,b], Yucheng Liu [b], Qingfeng Chen [a,b,c], Shuai Wei [a,b], Xuewei Li [b,*]

[a] *School of Resource and Environment, Nanchang University, Nanchang 330031, Jiangxi, PR China*
[b] *Ganjiang Innovation Academy, Chinese Academy of Sciences, Ganzhou 341000, China*
[c] *School of Public Health and Management, Nanchang Medical College, Nanchang 330052, Jiangxi, China*

Received 16 August 2022; accepted 3 December 2022
Available online 9 December 2022

KEYWORDS

Modified kaolin;
Adsorption;
Lanthanum;
Magnesium;
Rare earth recovery

Abstract As the world's demand for rare earths soars, the supply of rare earths is in danger of being depleted. The recycling rate of rare earth is only 1 % of all rare earth. Therefore, the recovery of rare earth is crucial and challenging. A phosphoric acid modified kaolin (P-K) was prepared by a simple mechanochemical method, and the selective recovery of rare earth element lanthanum (La) was studied. The P-K was characterized and analyzed by SEM, EDS, and FT-IR. Additionally, the different modification conditions of P-K preparation such as milling speed, time, and mass ratio of H_3PO_4/kaolin on La adsorption were investigated, and the effects of operating conditions such as solution initial pH, adsorption time, and adsorbent concentration on La adsorption were studied. The adsorption behavior of La by P-K was consistent with the Langmuir isothermal adsorption model with a saturated adsorption capacity of 18.55 mg/g, and the adsorption kinetics accorded with the pseudo-second-order kinetic model. Additionally, La in the mixture of La and magnesium (Mg) can be selectively adsorbed through P-K, while the adsorption rate of Mg is almost 0. P-K load with La could be eluted by 0.03 mol/L HCl, and the elution rate of La can reach 99.9 %.

* Corresponding authors.
E-mail addresses: kaibo0423@foxmail.com (K. Hu), tcchen21@gia.cas.cn (T. Chen), kli20@gia.cas.cn (K. Li), ycliu21@gia.cas.cn (Y. Liu), swei21@gia.cas.cn (S. Wei), xwli@gia.cas.cn (X. Li).
Peer review under responsibility of King Saud University.

Production and hosting by Elsevier

https://doi.org/10.1016/j.arabjc.2022.104498

As a result, this study demonstrates a method for the recovery of La from rare earth wastewater.

1. Introduction

Rare earth mines produce many low concentrations of rare earth wastewater during processing and smelting, which is prominent in volume and accompanied by considerable absolute values of rare earth content. Therefore, recovering rare earths from wastewater has significant value (Cao et al., 2021, Kegl et al., 2020, Liu et al., 2021). However, the recovery of rare earths is complicated due to the low concentration of rare earths in wastewater (Lee et al., 2021, Yang et al., 2022). On the one hand, rare earth ions in wastewater create heavy metal contamination problems that need to be removed. On the other hand, ammonium sulfate mining was gradually abandoned due to the ammonia nitrogen pollution problems, which was replaced by magnesium (Mg) salts leaching process (Li et al., 2022). In the current rare earth separation process, Mg as the main impurity widely exists in rare earth wastewater. Therefore, it has essential significance from Mg-containing wastewater efficient selective recovery of rare earths. Lanthanum (La) is one of the rare earth elements with high content in wastewater, which is widely used in metallurgy, glass, agriculture, biology, and other fields. Currently, the recovery of La is often performed by precipitation and solvent extraction technology (Ni et al., 2020, Nkinahamira et al., 2021), which leads to the generation of large amounts of acid-alkali wastewater and the use of volatile organic solvents, which not only damages the surrounding vegetation and causes severe environmental pollution, but also affect the lives of nearby residents. Therefore, it is necessary to develop a new, clean and efficient method for La recovery.

Solvent extraction (Dong et al., 2016, Hu et al., 2021, Zhou et al., 2021), membrane separation (Elbashier et al., 2021, Wang et al., 2020), precipitation (Balinski et al., 2020, de Vasconcellos et al., 2004), ion exchange (Stinn and Allanore, 2022), and adsorption methods (Adekanmbi et al., 2019, Borst et al., 2020, Smith et al., 2016, Tian et al., 2009, Zhao et al., 2017) are often used for the recovery of rare earth elements from wastewater. Compared with other technologies, adsorption is widely used for the recovery of rare earth elements from wastewater because of its low cost, wide range of applications and easy of operation. For example, Smith et al. reported the adsorption of pyrolysis waste tire carbon black on the mixture of light rare earth elements (Y, La, Ce, Nd, and Sm) (Smith et al., 2016). Ogata et al. developed a silica gel adsorbent with immobilized diethylene glycolic acid ligand (EDASiDGA) for selective recovery of rare earth elements Nd and Dy from acidic solutions (Ogata et al., 2016). Callura et al. investigated the capability of adsorbent silica particles functionalized with three different ligands-phosphonoacetic acid (PAA), N,*N*-bisphosphono (methyl)glycine (BPG) and diethylenetriaminepentaacetic dianhydride (DTPADA)-to selectively adsorb REE from acidic to circumneutral aqueous brine solutions in equilibrium conditions (Callura et al., 2018). Kusrini et al. studied the adsorption of La in an aqueous solution by pectin extracted from durian peels (Kusrini et al., 2018). However, there have been no report on the selective recovery of La from Mg-containing wastewater.

Kaolin is a low-cost clay adsorbent commonly found in nature with an ionic crystal structure, and its chemical composition is $Al_2SiO_5(OH)_4$. Kaolin is often used as a raw material for the development of solid-phase adsorbents and is widely used in metal ion adsorption and wastewater treatment because of its cheap price, easy availability, strong adsorption performance, and environmental friendliness (Chen et al., 2007, Jordao et al., 2009, Nandi et al., 2009, Zaman et al., 2002). For instance, Li et al. (Li et al., 2021) reported theoretical research on the adsorption mechanism of kaolin on $PbCl_2/CdCl_2$ during the process of garbage pyrolysis. Chen et al. discussed the adsorption mechanism of cadmium by the base surface of Kaolin (Chen et al., 2022). Xu et al. investigated the adsorption and interaction mechanisms of Chi-g-P(AM-DMDAAC) assisted settling of kaolin in a two-step flocculation process (Xu et al., 2022), Qiu et al. studied the adsorption of kaolin (001) surface hydration [$Lu(OH)_2$] and La through DFT theory research (Qiu et al., 2021, Qiu et al., 2022), and Guo et al. reported the experimental and molecular dynamics of kaolin-humic acid composites on glyphosate adsorption (Guo et al., 2021). However, relatively few research have been conducted on the recovery of rare earths by modified kaolin. Therefore, accelerating and strengthening the utilization of this inexpensive kaolin and developing kaolin adsorption materials with high adsorption properties for La are critical components for achieving sustainable industrial development and protecting the environment.

In this work, the kaolin was modified with H_3PO_4 using a mechanochemical method, which allowed a large amount of phosphates were combined with kaolin and greatly improved its adsorption properties. The morphology of P-K was characterized and analyzed by X-ray diffractometer (XRD) and scanning electron microscope (SEM), and a series of experiments were conducted to investigate the adsorption properties of P-K on La and the separation properties of La and Mg. Additionally, the adsorption mechanism of P-K on La was studied. A new process for the recovery of La from Mg-containing wastewater is proposed.

2. Experimental materials and methods

2.1. Chemicals and reagents

Phosphoric acid (H_3PO_4, ≥85 %), hydrochloric acid (HCl, ≥85 %), lanthanum chloride($LaCl_3$, ≥99.9 %), lanthanum nitrate($La(NO_3)_3$, ≥99.9 %), lanthanum sulfate($La_2(SO_4)_3$, ≥99.9 %) and magnesium chloride($MgCl_3$, ≥99.9 %) were purchased from Aladin Co., ltd. All reagents were analytically pure without further purification. Kaolin was kindly provided by a mine in southern China, and its XRD and XRF characterization is shown in Fig. S1 and Table S1.

2.2. Preparation

2 g of kaolin and a certain quality of H_3PO_4 were mixed and ground by a planetary ball mill equipped with two corundum grinding tanks (effective volume of about 100 cm^3, a diameter of 5.5 cm and height of 5 cm) and 16 zirconia balls (diameter of 2 × 2 cm, diameter of 8 × 1.5 cm, and diameter of 6 × 1 cm) with the weight ratio of ball-to-material equal to 75:1. The range of modification conditions were milling speed of 150–400 rpm, milling time of 0–120 min, and mass ratio of H_3PO_4/kaolin of 0–15 %.

2.3. Characterization

The crystal structure of P-K was analyzed by XRD (D8 Advance, Bruker AXS). The dried samples were tested by the powder wafer method and copper target radiation method, and XRD experiments were performed between 5° and 70°(2θ) with a step size of 0.02° and a measuring time of 0.15 s per step.

The surface morphology of P-K was tested by SEM (CLARA GMH microscope), and before the test, the sample was sprayed with gold. The characteristics of surface groups and valence bonds of the samples were determined by Fourier Transform Infrared Spectrometer (FTIR, iD7, Thermo Fisher Scientific) and the samples was prepared by mixing the dried samples with KBr at a ratio of 1:100 (mass ratio), and then the mixture was pressed into pellets. All spectra were collected in the wavelength range of 4000–400 cm^{-1}. The phosphorus in the solution was detected by an ultraviolet spectrophotometer (TU-1901) to determine the binding degree of the H_3PO_4 and the kaolin. All experiments were carried out at a room temperature of 298.15 K. The Brunauer-Emmett-Teller (BET) specific surface areas analysis were measured with Micromeritics instrument ASAP 2460. The zeta potential of this P-K was measured by the nanometer particle size potential analyzer (Zetasizer Pro).

2.4. Adsorption and elution experiments

A certain mass of P-K was stirred in 100 mL of the solution containing a certain concentration of metal ions, and then 10 mL of the mixed solution was centrifuged, and the concentration of metal ions in the supernatant after centrifugation was detected by ICPE-9000 (Shimadu, Japan). The elution experiments of P-K loaded with metal ions were carried out with different concentrations of hydrochloric acid solution (0 ~ 0.1 mol/L). Ammonium molybdate and ascorbic acid were used as phosphorus-based chromogenic reagents, and the content of phosphorus in the solution was measured by ultraviolet–visible spectrophotometer (TU-1901) with wavelength of 700 nm. The metal ion concentrations were analyzed and the adsorption efficiency (A), the adsorption capacity (q_t), and the elution efficiency (E) were calculated by the following equations:

$$A(\%) = \frac{C_i - C_f}{C_i} \tag{1}$$

$$q_t = \frac{(C_i - C_f)}{m} \times \frac{V}{M} \tag{2}$$

$$E(\%) = \frac{V \times C_f}{m \times q_e} \tag{3}$$

where the C_i and C_f represent the initial and final concentration of metal ions. V stands for the volume of solution, and m is the weight of the adsorbent. M represents the molar mass of metal ion. q_t and q_e are the adsorption capacity at the anytime t and adsorption equilibrium.

2.5. Adsorption kinetics and isothermal adsorption

The evaluation of the adsorption kinetics of La by P-K is based on pseudo- first-order model (4) and pseudo-second-order model (5) (Smith et al., 2016, Tian et al., 2009).

The pseudo-first-order model is as follows:

$$\ln(q_e - q_t) = lnq_e - \left(\frac{K_1}{2.303}\right)t \tag{4}$$

The pseudo-second-order kinetic model can be expressed as:

$$\frac{t}{q_t} = \frac{1}{K_2 q_{e^2}} + \frac{t}{q_e} \tag{5}$$

where q_t and q_e represent the adsorption capacity of La by P-K at the anytime t and adsorption equilibrium, respectively. K_1 is the rate constant of the pseudo-first-order equation, and K_2 is the rate constant of pseudo-second-order equation.

The Langmuir isotherm model and the Freundlich isotherm model were applied to fit the adsorption data and they are expressed by the following equations (6) and (7) (Smith et al., 2016, Tian et al., 2009):

The linear form of Langmuir adsorption isotherm is given as:

$$\frac{C_e}{q_e} = \frac{C_e}{q_m} + \frac{1}{K_L q_m} \tag{6}$$

The linear fitting equation of Freundlich adsorption isotherm is as follows:

$$lnq_e = \frac{1}{n}(lnC_e) + lnK_F \tag{7}$$

Where K_L is the Langmuir equilibrium constant, which is used to measure the affinity between adsorbate and adsorbent. q_m represents the saturated adsorption capacity. C_e is the equilibrium concentration of La in solution. K_F stands for the Freundlich equilibrium constant, which represents the adsorption ability. and n is a constant, which represents the adsorption intensity.

3. Results and discussion

3.1. Effect of phosphoric acid modification on surface properties of kaolin

The crystal phase of kaolin gradually disappeared after ball milling (Fig. 1a), which indicates that the crystal structure of kaolin has been transformed into amorphous state at a high speed, and it still exists in the form of crystal phase due to the relative stability of quartz phase,. It is observed that the adsorption performance of La by raw kaolin, kaolin modified without H_3PO_4 and P-K. It can be found that kaolin modified without H_3PO_4 has almost no adsorption effect on La, and the adsorption efficiency of P-K on La can reach 88.4 % under the same conditions, which reveals that the addition of H_3PO_4 greatly improves the adsorption performance of La. Addiyionally, the results reveal that the adsorption of La increased rapidly with the increase of adsorption time in the early stage, which could be attributed to the large amount of exchangeable H^+ on the surface of P-K, and La is easy to exchange with it. The exchangeable H^+ decreases with the prolongation of the adsorption time, resulting in a decrease in the mass transfer driving force, and then the adsorption efficiency of P-K on La begins to decrease until the adsorption equilibrium is reached.

The crystal phases of kaolin in the samples at different milling speeds were analyzed by XRD. The characteristic peaks of kaolinite in the sample weakened with the increase of milling speed (Fig. 2), which indicates that the H_3PO_4 and kaolin combine into an amorphous structure. In addition, the morphology of kaolin at different ball milling speeds was compared and analyzed by SEM, and Fig. 3a reveals that kaolin before milling shows a regular layered structure, while the

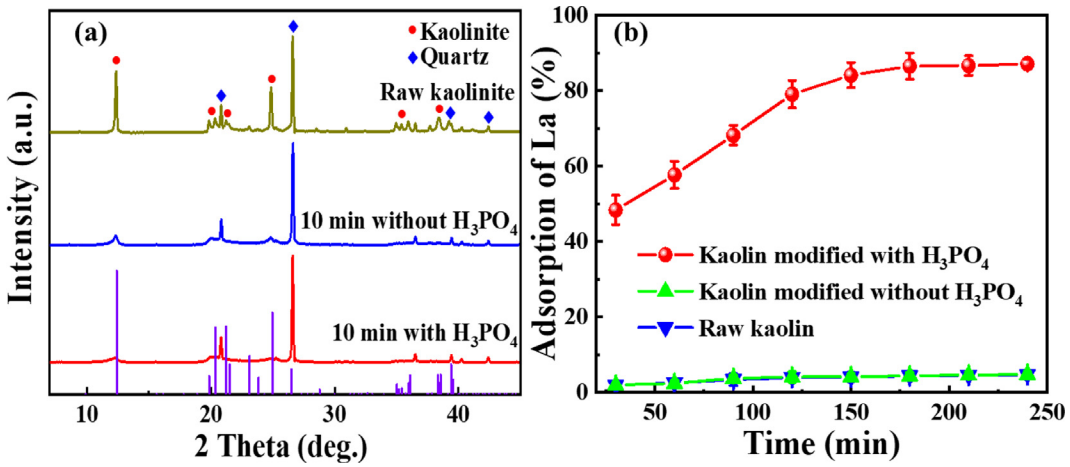

Fig. 1 (a) XRD patterns of the kaolin before and after modification, (b) and the adsorption properties of La, (milling speed of 400 rpm, milling time of 10 min, mass ratio of 10 % of H_3PO_4/kaolin) [La] = 30 mg/L, [P-K] = 2 g/L, initial pH 7.0.

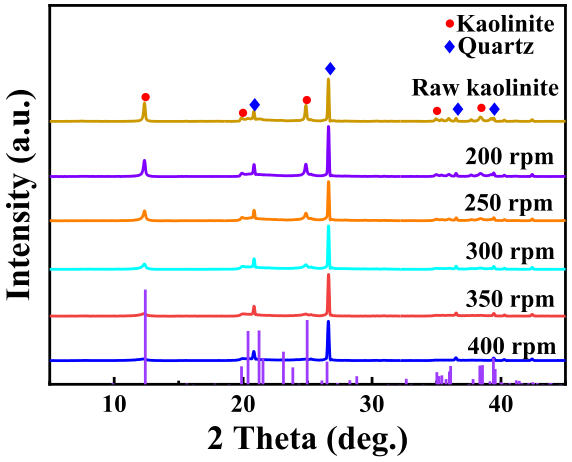

Fig. 2 XRD characterization of P-K under different milling speeds, milling time of 10 min, mass ratio of H_3PO_4/kaolin = 10 %.

kaolin samples in Fig. 3(b, c, d) are heavily aggregated. With the increase of grinding speed, the kaolin particles become finer, which is a normal phenomenon after the action of mechanical force.

The N_2 adsorption–desorption isotherms and pore size distribution curves for raw kaolin and P-K are presented in Fig. S2. The GC-0.25Ag@BiOCl exhibits the type-III isotherm patterns, and the specific surface area of P-K is significantly increased to 20 m^2/g after modification, suggesting that P-K has excellent adsorption performance.

3.2. Effect of different modification conditions on the performance of La adsorption

The milling speed and time are the main factors that determine whether H_3PO_4 can be stably loaded on the kaolin. The milling speed and time are too low to load H_3PO_4 onto kaolin, and too high milling speed and time will destroy the structure of kaolin, resulting in complete immobilization of free H^+ in H_3PO_4, which cannot be exchanged. Fig. 4a indicates the dissolution of phosphorus in the solution gradually decreases with the increase of the milling speed, when the milling speed is 400 rpm, the dissolution of phosphorus is almost 0, and the adsorption efficiency of La can reach 88.4 %. Therefore, 400 rpm is selected as the optimal milling speed in the following experiments. As can be seen from Fig. 4b that the adsorption efficiency of La decreases with the increase of milling time, and when the milling time is 5 min, the adsorption efficiency of La can reach 99.4 %, but about 10 ppm phosphoric is dissolved in the solution, which reveals that H_3PO_4 is not completely loaded on the kaolin. When the milling time is more than 10 min, the dissolution of phosphorus in the solution is almost 0. Therefore, 10 min is chosen as the optimal milling time in the following experiments.

The mass ratio of H_3PO_4/kaolin has a direct effect on the modification effect of kaolin, too little mass ratio of H_3PO_4/kaolin will cause a limited amount of commutative free H^+, which will limit the adsorption performance of P-K. Too high mass ratio of H_3PO_4/kaolin will lead to dissolution of excess phosphoric acid. Fig. 4 indicates that the adsorption efficiency of La gradually increases with the increase of mass ratio of H_3PO_4/kaolin, and when the mass ratio of H_3PO_4/kaolin is greater than 10 %, the phosphorus dissolves in the solution. Therefore, in the next experiment, the mass ratio of H_3PO_4/kaolin is chosen to be 10 % in order to avoid the waste of H_3PO_4.

3.3. Effect of operating conditions on the performance of La adsorption

Industrial feedstocks containing La are usually not present in neutral form, so it is necessary to investigate the effect of pH on the adsorption of La by P-K. In this experiment, the adsorption effect of P-K on La at initial pH values of 1 to 7.5 was investigated. It is observed that the adsorption efficiency of La by P-K gradually increases with the increase of initial pH, indicating that the H^+ in the solution inhibit the exchange process of La and free H^+ in P-K to a certain extent, which also lead to poor adsorption performance of P-K on La under acidic conditions. Additionally, the dissolution of phosphorus in the solution increases with the decrease of the initial

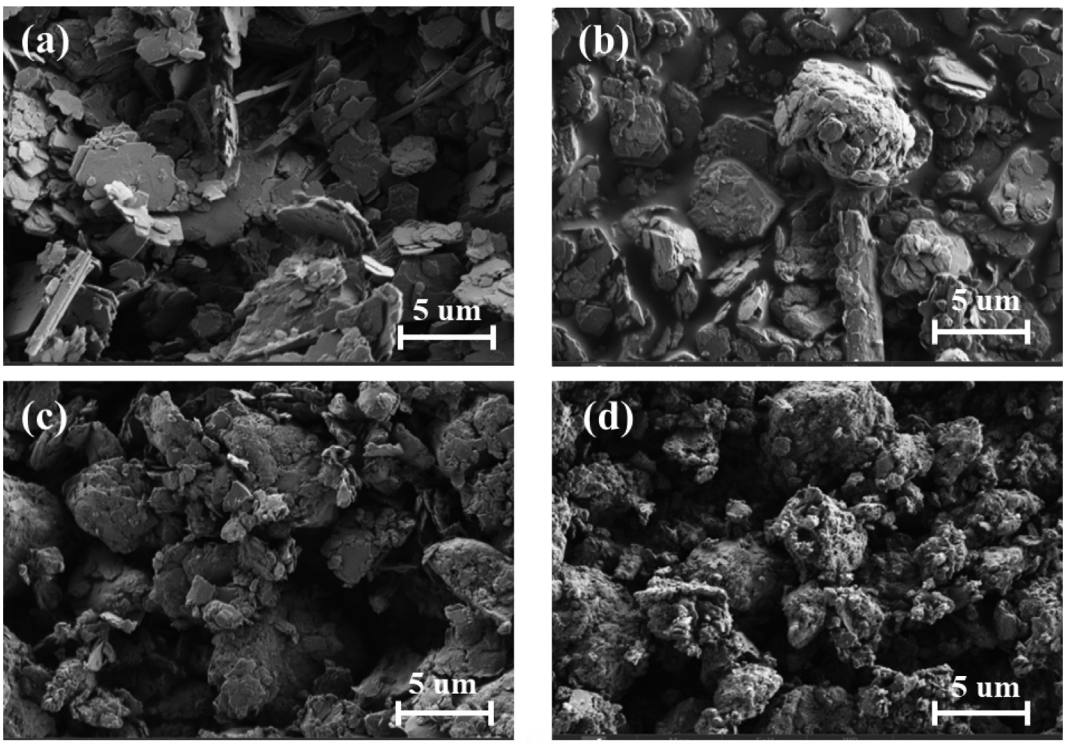

Fig. 3 SEM images of (a) Raw kaolin, (b)P-K of 150 rpm, (c) P-K of 250 rpm, (d) P-K of 400 rpm.

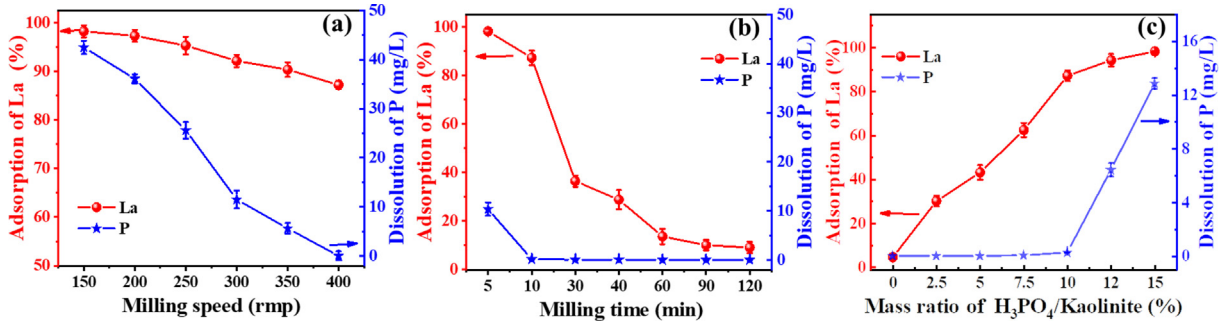

Fig. 4 Effect of (a) milling speed, (b) milling time, and (c) mass ratio of H_3PO_4/kaolin on La adsorption. (a: milling time of 10 min, a mass ratio of 10 % of H_3PO_4/kaolin, b: milling speed of 400 rpm, a mass ratio of 10 % of H_3PO_4/kaolin, c: milling speed of 400 rpm, milling time of 10 min) [La] = 30 mg/L, [P-K] = 2 g/L, initial pH 7.0.

pH, and this side reaction lead to the poor stability of P-K under strongly acidic conditions. Additionally, it is observed from Fig. S3 that the isoelectric point of P-K is located near pH = 6, and when the pH is lower or higher than the isoelectric point, the surface of the P-K particles is positively charged and negatively charged, respectively, so the adsorption efficiency of P-K on La increases with the increase of pH. When the pH is 2, the decrease in zeta potential of P-K may be due to reduced stability of P-K under acidic conditions. Therefore, a pH value between 6 and 7 is chosen in the next experiment.

Fig. 5b reveals that the adsorption rate of La increases with the increase of P-K concentration, and 2 g/L P-K is selected as the research object in order to better reflect the adsorption behavior of La by P-K. Additionally, the initial concentration of La is an critical factor affecting the adsorption capacity and P-K. The concentration gradient of the P-K surface and the adsorbed substance increases with the increase of the initial concentration of La, and the high concentration gradient leads to high mass transfer dynamics. Therefore, the adsorption efficiency of La by P-K under different initial concentration conditions is tested, and it is observed that the adsorption capacity of La by P-K increases with the increase of the initial concentration of La. When the initial concentrations of La are 30 mg/L, 40 mg/L, and 50 mg/L, the adsorption capacity of La by P-K are 11.24 mg/g, 12.35 mg/g, and 14.11 mg/g, respectively. The results demonstrate that the high concentration mass transfer driving force is conducive to the increase of P-K adsorption capacity, but its equilibrium time increased. Therefore, the selection of La concentration is conducive to amplifying the advantages of the adsorbent, and to ensure high adsorption efficiency, a La concentration of 30 mg/L is selected for the next experiment.

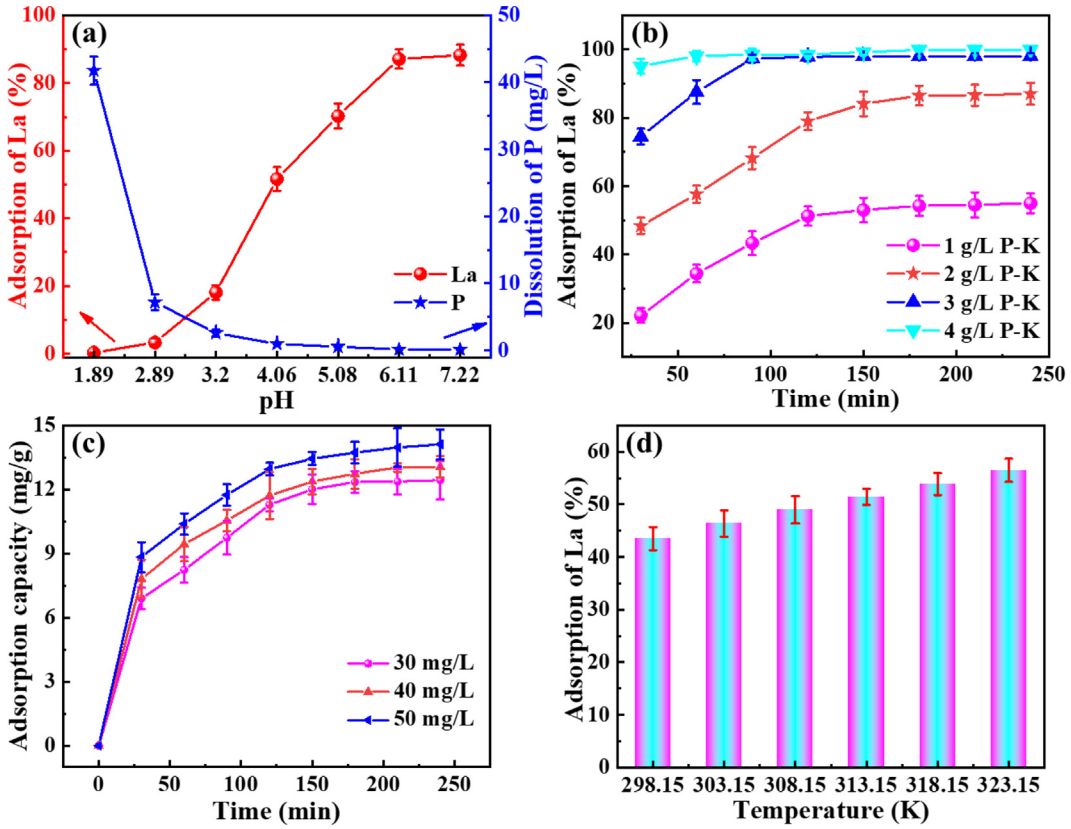

Fig. 5 (a) Effect of initial pH, (b) P-K concentration, (c) initial concentration of La, and (d) temperature on La adsorption.

To highlight the effect of temperature on La adsorption, 1 g/L of P-K is taken in a conical flask filled containing 30 mg/L La solution, and shaken at a constant temperature of 298.15–323.15 K for 3 h, respectively. The results are presented in Fig. 5d, the increase of temperature can promote the adsorption rate of La by P-K, and the reason may be that the increase of temperature makes La in the solution more active, which accelerates the adsorption efficiency and increases the adsorption capacity of P-K on La. The results demonstrate that the adsorption process is endothermic, and heating is conducive to the adsorption of La.

3.4. Adsorption mechanism

3.4.1. Adsorption kinetics

To investigate the adsorption kinetic characteristics of P-K on La, the adsorption of La in Fig. 5c is treated with a pseudo-first-order kinetic model and pseudo-second-order kinetic model, and the results are presented in Fig. 6. According to the fitted data, the theoretical adsorption values (q_{cal}), kinetic adsorption rates (K_1, K_2), and fitting coefficients (R^2) of the pseudo-first-order kinetic equation and the pseudo-second-order kinetic equation can be calculated by slope and intercept, and the specific results are shown in Table 1. Fig. 6a reveals that the determined coefficients obtained according to the pseudo-first-order kinetic equation are 0.98, 0.98, and 0.97 when the La concentrations are 30 mg/L, 40 mg/L, and 50 mg/L, respectively. The results of Fig. 6b reveal that the linear correlation coefficients obtained according to the pseudo-second-order kinetic model are 0.99, 0.99, 0.99, respectively, and the adsorption of La by P-K is more consistent with the pseudo-second-order kinetic model, and the q_{cal} calculated are 11.90, 12.82 and 14.92 mg/g, respectively, which are closer to the actual saturation adsorption capacity (q_{exp}). The results of adsorption kinetics demonstrate that the adsorption process of La by P-K is dominated by chemical adsorption, which further reveal that the adsorption of La is realized by exchanging H^+ on the surface of P-K. Additionally, when the initial concentrations of La are 30 mg/L, 40 mg/L, and 50 mg/L, respectively, the K_2 values are 0.0052 g/(mg·min), 0.0048 g/(mg·min) and 0.041 g/(mg·min), and the pseudo-second-order kinetic model constant K_2 represent that the kinetic rate gradually decreases with the increase of the initial La concentration.

3.4.2. Adsorption isotherm

The Langmuir and Freundlich adsorption isotherm models were used to fit the variation curves of equilibrium concentrations C_e and q_e at different temperatures in Fig. 7. The theoretical saturated adsorption capacity (q_{max}) and adsorption equilibrium constant (b) can be calculated according to the intercept and slope in Langmuir fitting equation, while the adsorption coefficient (KF) and adsorption intensity characteristic constant (n) can be obtained according to Freundlich adsorption isotherm equation, and the results are presented in Table 2. It can be seen from Fig. 8(a, b) that the adsorption of La by P-K is more consistent with the Langmuir adsorption isotherm equation with the fitted coefficients R^2 of 0.99, which are far greater than the fitting coefficients obtained by Freundlich adsorption isotherm equation, and their values are 0.92, 0.96 and 0.98, respectively. The q_{max} at different temper-

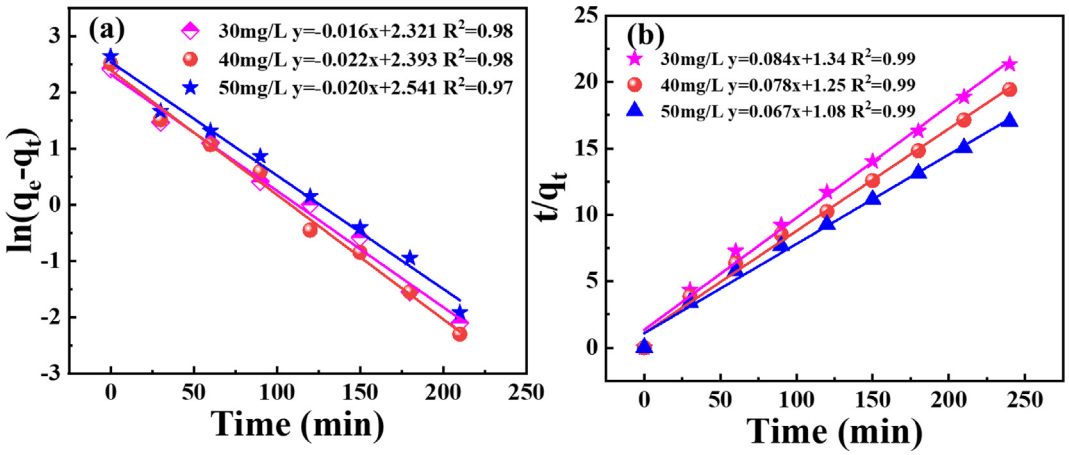

Fig. 6 (a) Preudo-first-order kinetic model and (b) pseudo-second-order kinetic model of La adsorbed by P-K.

Table 1 Estimated adsorption kinetic parameters for La by pseudo-first-order kinetic model and pseudo-second-order kinetic model.

C_{La}^{+} (mg/L)		30	40	50
q_{exp} (mg/g)		11.24	12.35	14.11
pseudo-first-order kinetic model	q_{cal} (mg/g)	10.18	10.27	12.69
	K_1 (1/min)	0.03	0.05	0.04
	R^2	0.98	0.98	0.97
pseudo-second-order kinetic model	q_{cal} (mg/g)	11.90	12.82	14.92
	K_2 (g/(mg·min)	0.0052	0.0048	0.0041
	R^2	0.99	0.99	0.99

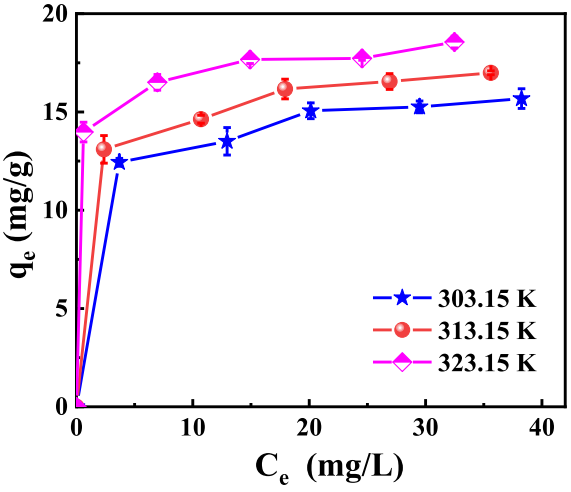

Fig. 7 Effect of temperature and La concentration on adsorption capacity of La.

atures fitted by the Langmuir adsorption isotherm equation are 16.39 mg/g, 17.54 mg/g, and 18.86 mg/g, respectively, which is closer to the actual saturation adsorption amounts (15.67 mg/g, 16.99 mg/g, and 18.55 mg/g), which demonstrates that the adsorption mechanism of La by P-K can be described by Langmuir adsorption isothermal formula. The adsorption process is dominated by chemical adsorption and exhibits the characteristics of single molecular layer adsorption. The 1/n value obtained from Freundlich's empirical formula is less than 0.5, which indicates that the adsorption of La by P-K is relatively easy to carry out in this temperature range.

3.4.3. Analysis of the adsorption process

For the raw kaolin, frequency bands at 3696 cm^{-1} and 3622 cm^{-1} can be assigned to the inner surface hydroxyl group and the inner hydroxyl group, respectively. They are connected to aluminum in aluminum-oxygen octahedrons (Cheng et al., 2021, Deng et al., 2020). Frequency ranges of 796–692 cm^{-1} can be attributed to O—Si—O bending vibration (Cheng et al., 2019, Nwosu et al., 2018). For the kaolin modified, the surface functional groups of kaolin have undergone significant changes. The frequency bands at 3696 $cm^{-1}$and 3622 cm^{-1} are significantly weakened, indicating the process of dihydroxy and amorphous material formation. In addition, the strong peak of the P—O group appears at 1037 cm^{-1}, which reveals that H_3PO_4 binds to kaolin, and significant bending vibrations appear at the peak at 1638 cm^{-1}, which suggests that the hydroxyl groups in the structure may have combined with the hydrogen from H_3PO_4 to form water (Lei et al., 2018). After the adsorption reaction, the P—O group that appears at 1037 cm^{-1} has obvious stretching vibration, which proves that the adsorption process is the reaction of phosphate and La in the P-K.

Fig. 9a shows that the pH value in the solution gradually decreases with the increase of the adsorption time, which confirms that the adsorption of La by P-K is essentially the ion exchange reaction between La ions in the solution and the H ions from P-K.

3.5. Effect of anions on La adsorption and selective adsorption of La from Mg-containing solutions

The adsorption of P-K on different La salt solutions is the key point to investigate the applicability of P-K, so three representative inorganic La salt solutions are selected as experimental objects, which are $LaCl_3$, $La(NO_3)_3$, and $La_2(SO_4)_3$. As presented in Fig. 10a, the adsorption capacity of P-K for the three La salts are about 12 mg/L, indicating that P-K has a wide range of application.

Table 2 Model parameters for the adsorption of La on P-K.

Temperature (K)	Langmuir Model Parameters				Freundlich Model Parameters		
	q_{max} (mg/g)	q_e (mg/g)	KL	R^2	1/n	K_F	R^2
303.15	16.39	15.67	0.56	0.99	0.10	0.86	0.92
313.15	17.54	16.99	0.74	0.99	0.09	0.90	0.96
323.15	18.86	18.55	0.94	0.99	0.07	0.98	0.98

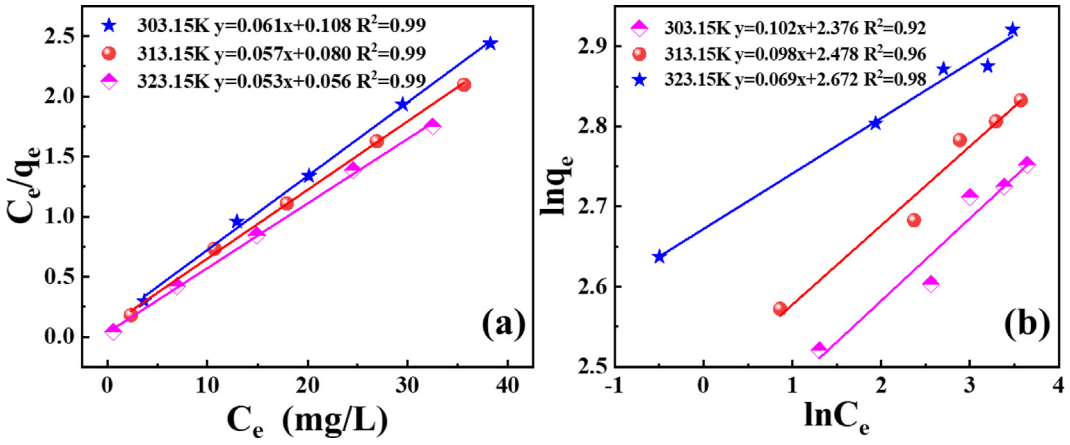

Fig. 8 (a) Langmuir adsorption isotherm equation fitting, (b) Freundlich adsorption isotherm equation fitting.

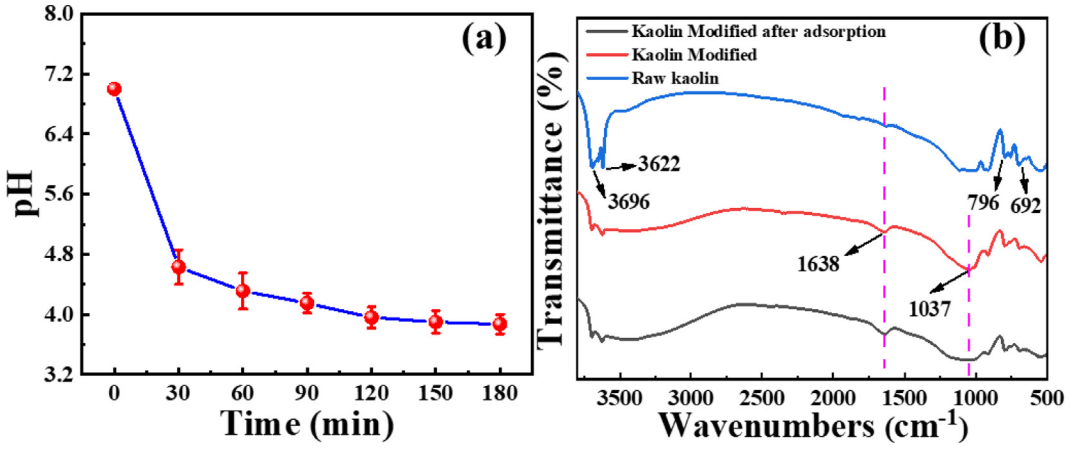

Fig. 9 (a) The pH change during adsorption and (b) FT-IR characterization of samples.

The specific adsorption capacity of the P-K is evaluated by selective experiments in a mixed solution (La, Mg). From Fig. 10b, it is observed that P-K has superior selective performance for La, which is due to the pecific chelation between phosphate groups on the surface of P-K and La of solutions, and thus P-K has a specific selection function for La. The results confirm that P-K can achieve selective separation of La and Mg, which has a high application value.

3.6. Elution of La

It can be founded from Fig. 11 that the elution efficiency of La increases significantly and remaines stable as the hydrochloric acid concentration increases in the range of 0–0.05 mol/L. When the hydrochloric acid concentration is 0.03 mol/L, the elution efficiency of La can reach 99.9 %. The results indicate that La on P-K could be easily eluted under low acid condi-

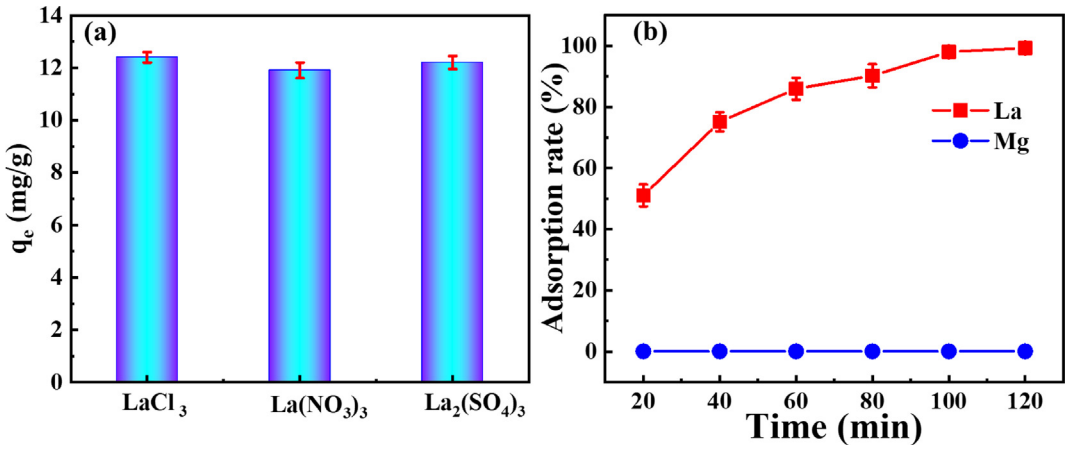

Fig. 10 (a) Effect of anions on La adsorption and (b) selective separation of La and Mg, (a: [P-K] = 2 g/L, [La] = 30 mg/L, initial pH = 7, (b): [P-K] = 3 g/L, [La] = [Mg] = 30 mg/L, initial pH = 7).

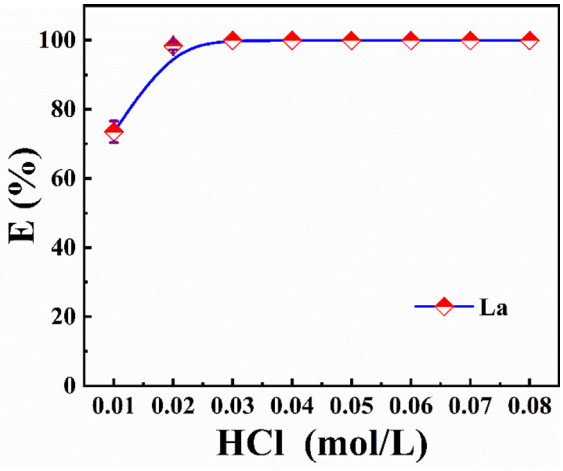

Fig. 11 Elution of the P-K loaded with La, [P-K] = 2 g/L, [La] = 30 mg/L.

tions, which further demonstrates its superior desorption performance.

4. Conclusion

In summary, P-K was synthesized by mechanochemical method with H_3PO_4 and kaolin as raw materials, which was simple to operate, environmentally friendly, easy to obtain raw materials, low cost, and wide range of applications. The effects of key parameters of P-K preparation such as milling time and milling speed on La adsorption were investigated, and the effects of initial pH value, contact time, initial concentration of La, P-K dosage and other operating conditions on La adsorption were studied. The results showed that the optimal modification parameters and operating conditions were as follows: it was ground with 400 rpm balls for 10 min, accompanied by H_3PO_4/kaolin with a mass ratio of 10 %, the optimal pH of the solution was 7 ± 0.3, and the adsorption process of La was endothermic. In addition, the adsorption behavior of La on P-K was consistent with the Langmuir isothermal adsorption model, with a maximum saturation adsorption capacity of 18.55 mg/g. The adsorption kinetics followed the pseudo-second-order kinetics model, and the adsorption process of La was accompanied by proton exchange. Selective experiments have shown that P-K can selectively absorb La of mixture solution while having almost no adsorption effect on Mg. Elution experiments showed that the P-K loaded with La can be eluted with 0.03 mol/L HCl, and the elution rate of La was 99.9 %. In addition, this study shows that P-K is a promising strategy for the separation, recovery, and enrichment of rare earth La in wastewater.

Declaration of Competing Interest

The authors declare that they have no known competing financial interests or personal relationships that could have appeared to influence the work reported in this paper.

Acknowledgment

This work was supported by a grant from the Research Projects of Ganjiang Innovation Academy, Chinese Academy of Sciences (E055ZA01), and the China National Key R&D Program (Grant No. 2022YFB3504303).

Appendix A. Supplementary material

Supplementary data to this article can be found online at https://doi.org/10.1016/j.arabjc.2022.104498.

References

Adekanmbi, E.O., Giduthuri, A.T., Waymire, S., Srivastava, S.K., 2019. Utilization of dielectrophoresis for the quantification of rare earth elements adsorbed on cupriavidus necator. ACS Sustain. Chem. Eng. 8 (3), 1353–1361. https://doi.org/10.1021/acssuschemeng.9b03878.

Balinski, A., Wiche, O., Kelly, N., Reuter, M.A., Scharf, C., 2020. Separation of rare earth elements from contaminants and valuable components by in-situ precipitation during the hydrometallurgical processing of eudialyte concentrate. Hydrometall. 194,. https://doi.org/10.1016/j.hydromet.2020.105345 105345.

Borst, A.M., Smith, M.P., Finch, A.A., Estrade, G., Villanova-de-Benavent, C., Nason, P., Geraki, K., 2020. Adsorption of rare earth elements in regolith-hosted clay deposits. Nat Commun. 11 (1), 4386. https://doi.org/10.1038/s41467-020-17801-5.

Callura, J.C., Perkins, K.M., Noack, C.W., Washburn, N.R., Dzombak, D.A., Karamalidis, A.K., 2018. Selective adsorption of rare

earth elements onto functionalized silica particles. Green Chem. 20 (7), 1515–1526. https://doi.org/10.1039/c8gc00051d.

Cao, Y., Shao, P., Chen, Y., Zhou, X., Yang, L., Shi, H., Luo, X., 2021. A critical review of the recovery of rare earth elements from wastewater by algae for resources recycling technologies. Resour. Conserv. Recycl. 169,. https://doi.org/10.1016/j.resconrec.2021.105519 105519.

Chen, Y., Liu, S., Wang, G., 2007. A kinetic investigation of cationic starch adsorption and flocculation in kaolin suspension. Chem. Eng. J. 133 (1–3), 325–333. https://doi.org/10.1016/j.cej.2007.02.019.

Chen, G., Zhao, H., Li, X., Xia, S., 2022. Theoretical insights into the adsorption mechanism of Cd(II) on the basal surfaces of kaolinite. J. Hazard Mater. 422,. https://doi.org/10.1016/j.jhazmat.2021.126795 126795.

Cheng, Y., Xing, J., Bu, C., Zhang, J., Piao, G., Huang, Y., Xie, H., Wang, X., 2019. Dehydroxylation and structural distortion of kaolinite as a high-temperature sorbent in the furnace. Minerals 9 (10), 587. https://doi.org/10.3390/min9100587.

Cheng, H., Huang, Y., Zhu, Z., Dong, L., Zha, J., Yu, M., 2021. Enhanced $PbCl_2$ adsorption capacity of modified kaolin in the furnace using a combined method of thermal pre-activation and acid impregnation. Chem. Eng. J. 414,. https://doi.org/10.1016/j.cej.2021.128672 128672.

de Vasconcellos, M.E., Queiroz, C.A.d.S., Abrão, A.d., 2004. Sequential separation of the yttrium—heavy rare earths by fractional hydroxide precipitation. J. Alloys Compounds 374 (1–2), 405–407. https://doi.org/10.1016/j.jallcom.2003.11.038.

Deng, C., Xie, X., Han, J., Tang, Y., Gao, J., Liu, C., Liang, S., 2020. A sieve-functional and uniform-porous kaolin layer toward stable zinc metal anode. Adv. Funct. Mater. 30 (21), 2000599. https://doi.org/10.1002/adfm.202000599.

Dong, Y., Sun, X., Wang, Y., Huang, C., Zhao, Z., 2016. The sustainable and efficient ionic liquid-type saponification strategy for rare earth separation processing. ACS Sustain. Chem. Eng. 4 (3), 1573–1580. https://doi.org/10.1021/acssuschemeng.5b01499.

Elbashier, E., Mussa, A., Hafiz, M., Hawari, A.H., 2021. Recovery of rare earth elements from waste streams using membrane processes: an overview. Hydrometall. 204,. https://doi.org/10.1016/j.hydromet.2021.105706 105706.

Guo, F., Zhou, M., Xu, J., Fein, J.B., Yu, Q., Wang, Y., Rong, X., 2021. Glyphosate adsorption onto kaolinite and kaolinite-humic acid composites: experimental and molecular dynamics studies. Chemosphere 263,. https://doi.org/10.1016/j.chemosphere.2020.127979 127979.

Hu, K., Gao, H., Nie, Y., Dong, H., Yan, J., Zhang, X., Li, F., 2021. Efficient selective separation of yttrium from holmium and erbium using carboxyl functionalized ionic liquids. Sep. Purif. Technol. 269,. https://doi.org/10.1016/j.seppur.2021.118774 118774.

Jordao, C.P., Fernandes, R.B., de Lima Ribeiro, K., de Souza Nascimento, B., de Barros, P.M., 2009. Zn(II) adsorption from synthetic solution and kaolin wastewater onto vermicompost. J. Hazard Mater. 162 (2–3), 804–811. https://doi.org/10.1016/j.jhazmat.2008.05.104.

Kegl, T., Kosak, A., Lobnik, A., Novak, Z., Kralj, A.K., Ban, I., 2020. Adsorption of rare earth metals from wastewater by nanomaterials: A review. J Hazard Mater. 386,. https://doi.org/10.1016/j.jhazmat.2019.121632 121632.

Kusrini, E., Wicaksono, W., Gunawan, C., Daud, N.Z.A., Usman, A., 2018. Kinetics, mechanism, and thermodynamics of lanthanum adsorption on pectin extracted from durian rind. J. Environ. Chem. Eng. 6 (5), 6580–6588. https://doi.org/10.1016/j.jece.2018.10.018.

Lee, Y., Ren, Y., Cui, M., Ma, J., Han, Z., Kwon, O., Khim, J., 2021. Rare earth real wastewater treatment by pilot scale using new concept continuous treatment process. Chemosphere 279,. https://doi.org/10.1016/j.chemosphere.2021.130523 130523.

Lei, Z., Cagnetta, G., Li, X., Qu, J., Li, Z., Zhang, Q., Huang, J., 2018. Enhanced adsorption of potassium nitrate with potassium cation on H_3PO_4 modified kaolinite and nitrate anion into Mg-Al layered double hydroxide. Appl. Clay Sci. 154, 10–16. https://doi.org/10.1016/j.clay.2017.12.040.

Li, J., Zhong, Z., Du, H., Li, Q., Wang, N., Zhao, H., Huang, J., 2021. Theoretical study on the adsorption mechanism of $PbCl_2/CdCl_2$ by kaolinite during municipal solid waste pyrolysis. Chemosphere 267,. https://doi.org/10.1016/j.chemosphere.2020.129184 129184.

Li, J., Lu, H., Ng, P.K., Pantazi, A., Ip, C.K.M., Jeong, K.J., Liang, H., 2022. A functional genomic approach to actionable gene fusions for precision oncology. Sci Adv. 8 (6), eabm2382. https://doi.org/10.1126/sciadv.abm2382.

Liu, X., Huang, L., Liu, Z., Zhang, D., Gao, K., Li, M., 2021. A novel, clean, closed-loop process for directional recovery of rare earth elements, fluorine, and phosphorus from mixed rare earth concentrate. J. Clean. Prod. 321,. https://doi.org/10.1016/j.jclepro.2021.128784 128784.

Nandi, B.K., Goswami, A., Purkait, M.K., 2009. Adsorption characteristics of brilliant green dye on kaolin. J Hazard Mater. 161 (1), 387–395. https://doi.org/10.1016/j.jhazmat.2008.03.110.

Ni, S., Chen, Q., Gao, Y., Guo, X., Sun, X., 2020. Recovery of rare earths from industrial wastewater using extraction-precipitation strategy for resource and environmental concerns. Miner. Eng. 151,. https://doi.org/10.1016/j.mineng.2020.106315 106315.

Nkinahamira, F., Alsbaiee, A., Wang, Y., Yang, X., Chen, T.-Y., Cao, M., Yu, C.-P., 2021. Recovery and purification of rare earth elements from wastewater and sludge using a porous magnetic composite of β-cyclodextrin and silica doped with PC88A. Sep. Purif. Technol. 266,. https://doi.org/10.1016/j.seppur.2021.118589 118589.

Nwosu, F.O., Ajala, O.J., Owoyemi, R.M., Raheem, B.G., 2018. Preparation and characterization of adsorbents derived from bentonite and kaolin clays. Appl. Water Sci. 8 (7), 195. https://doi.org/10.1007/s13201-018-0827-2.

Ogata, T., Narita, H., Tanaka, M., 2016. Adsorption mechanism of rare earth elements by adsorbents with diglycolamic acid ligands. Hydrometall. 163, 156–160. https://doi.org/10.1016/j.hydromet.2016.04.002.

Qiu, S., Wu, H., Yan, H., Li, X., Zhou, X., Qiu, T., 2021. Theoretical investigation of hydrated $[Lu(OH)_2]^+$ adsorption on kaolinite(001) surface with DFT calculations. Appl. Surf. Sci. 565,. https://doi.org/10.1016/j.apsusc.2021.150473 150473.

Qiu, S., Yan, H., Qiu, X., Wu, H., Zhou, X., Wu, H., Qiu, T., 2022. Adsorption of La on kaolinite (001) surface in aqueous system: A combined simulation with an experimental verification. J. Mol. Liq. 347,. https://doi.org/10.1016/j.molliq.2021.117956 117956.

Smith, Y.R., Bhattacharyya, D., Willhard, T., Misra, M., 2016. Adsorption of aqueous rare earth elements using carbon black derived from recycled tires. Chem. Eng. J. 296, 102–111. https://doi.org/10.1016/j.cej.2016.03.082.

Stinn, C., Allanore, A., 2022. Selective sulfidation of metal compounds. Nature 602 (7895), 78–83. https://doi.org/10.1038/s41586-021-04321-5.

Tian, S., Jiang, P., Ning, P., Su, Y., 2009. Enhanced adsorption removal of phosphate from water by mixed lanthanum/aluminum pillared montmorillonite. Chem. Eng. J. 151 (1–3), 141–148. https://doi.org/10.1016/j.cej.2009.02.006.

Wang, Y., Chen, L., Yan, Y., Chen, J., Dai, J., Dai, X., 2020. Separation of adjacent heavy rare earth Lutetium (III) and Ytterbium (III) by task-specific ionic liquid Cyphos IL 104 embedded polymer inclusion membrane. J. Membr. Sci. 610,. https://doi.org/10.1016/j.memsci.2020.118263 118263.

Xu, R., Zou, W., Wang, T., Huang, J., Zhang, Z., Xu, C., 2022. Adsorption and interaction mechanisms of Chi-g-P(AM-DMDAAC) assisted settling of kaolinite in a two-step flocculation process. Sci Total Environ. 816,. https://doi.org/10.1016/j.scitotenv.2021.151576 151576.

Yang, L., Geng, Y., Cui, D., Liu, Z., Xiong, Z., Pavlostathis, S.G., Luo, X., 2022. Corrected response surface methodology for

microalgae towards optimized ammonia nitrogen removal: A case of rare earth mining tailings wastewater in Southern Jiangxi. China. Journal of Cleaner Production. 343,. https://doi.org/10.1016/j.jclepro.2022.130998 130998.

Zaman, A.A., Tsuchiya, R., Moudgil, B.M., 2002. Adsorption of a low-molecular-weight polyacrylic acid on silica, alumina, and kaolin. J. Colloid Interface Sci. 256 (1), 73–78. https://doi.org/10.1006/jcis.2001.7941.

Zhao, F., Repo, E., Song, Y., Yin, D., Hammouda, S.B., Chen, L., Sillanpää, M., 2017. Polyethylenimine-cross-linked cellulose nanocrystals for highly efficient recovery of rare earth elements from water and a mechanism study. Green Chem. 19 (20), 4816–4828.

Zhou, J., Ma, S., Chen, Y., Ning, S., Wei, Y., Fujita, T., 2021. Recovery of scandium from red mud by leaching with titanium white waste acid and solvent extraction with P204. Hydrometall. 204,. https://doi.org/10.1016/j.hydromet.2021.105724 105724.